A high-efficiency regime for gas-phase terahertz lasers

Fan Wang[a,b,1], Jeongwon Lee[b], Dane J. Phillips[c], Samuel G. Holliday[c], Song-Liang Chua[d], Jorge Bravo-Abad[e], John D. Joannopoulos[b,f,1], Marin Soljačić[b,f], Steven G. Johnson[b,f,g,1], and Henry O. Everitt[h,i,1]

[a]Department of Mechanical Engineering, Massachusetts Institute of Technology, Cambridge, MA 02139; [b]Research Laboratory of Electronics, Massachusetts Institute of Technology, Cambridge, MA 02139; [c]IERUS Technologies, Huntsville, AL 35805; [d]Defense Science Organization National Laboratories, Singapore 118225 Singapore; [e]Departamento de Física Teórica de la Materia Condensada and Condensed Matter Physics Center, Universidad Autónoma de Madrid, 28049 Madrid, Spain; [f]Department of Physics, Massachusetts Institute of Technology, Cambridge, MA 02139; [g]Department of Mathematics, Massachusetts Institute of Technology, Cambridge, MA 02139; [h]Department of Physics, Duke University, Durham, NC 27708; and [i]Army Aviation & Missile Research, Development, and Engineering Center, Redstone Arsenal, AL 35898

We present both an innovative theoretical model and an experimental validation of a molecular gas optically pumped far-infrared (OPFIR) laser at 0.25 THz that exhibits 10× greater efficiency (39% of the Manley–Rowe limit) and 1,000× smaller volume than comparable commercial lasers. Unlike previous OPFIR-laser models involving only a few energy levels that failed even qualitatively to match experiments at high pressures, our ab initio theory matches experiments quantitatively, within experimental uncertainties with no free parameters, by accurately capturing the interplay of millions of degrees of freedom in the laser. We show that previous OPFIR lasers were inefficient simply by being too large and that high powers favor high pressures and small cavities. We believe that these results will revive interest in OPFIR laser as a powerful and compact source of terahertz radiation.

optically pumped far-infrared laser | terahertz source | continuous wave gas laser | laser modeling | rotational population inversion

For many years, optically pumped far-infrared (OPFIR) gas lasers were the most powerful sources of continuous-wave (CW) terahertz radiation (1–13), and such terahertz sources are crucial to a wide variety of sensing and imaging applications (14–16). They employ population inversions excited in molecule-specific rotational–vibrational transitions by a line-tunable CO_2 laser. By changing the gas, isotope, and CO_2 laser line, different transition frequencies could be made to lase, typically in meter-long cavities operated at low pressures (<0.1 Torr) and producing up to 100 mW in a manner that depended strongly on the rotational transition involved (https://www.edinst.com/products/; ref. 17). Initially, it was thought that low pressures and large cavities were required, but this produced a "vibrational bottleneck": diffusion-limited relaxation by molecule–wall collisions that filled the vibrational level and quenched any inversion above a maximum pressure, regardless of the pump intensity (2, 4, 6). It was subsequently discovered that OPFIR lasers could operate at pressures higher than this in smaller cavities, a result of collisional processes that excited high-energy vibrational levels and removed the bottleneck (7, 9). This breakthrough was never fully investigated or exploited, however, as it came at a time when new sources of terahertz radiation were emerging (18–20) and the use of OPFIR lasers was waning due to their supposed large sizes (e.g., 10 cm in diameter and 1 m in length) and low photon conversion efficiencies (e.g., 0.1–10%).

The advent of alternatives to line-tunable CO_2 lasers (21, 22) and the increasing need for powerful, narrowband sources of terahertz radiation are reviving interest in compact OPFIR lasers (13), whose full potential has never been fully understood because of the thousands of quantized states involved and the millions of collision cross-sections required to simulate its behavior adequately. In fact, all previous OPFIR-laser models involving only a few vibrational levels exhibited unphysical bottlenecking at high pressures and failed even qualitatively to match experiments (2–4, 13).

Here, we present both experiments and an innovative theoretical model that not only match at all pressures, but also exhibit unprecedented conversion efficiencies and device compactness. We solve deficiencies of earlier models by developing a far more complete theory for a compact OPFIR laser, using the prototypical molecular gas $^{13}CH_3F$ pumped by a line-tunable CO_2 laser (Fig. 1). Using no adjustable parameters, our model matches our experimental measurements (Fig. 2) with excellent accuracy, especially considering its sensitivity to many experimental variables. The critical part of our theory is an effective vibrational temperature that includes all accessible high-lying vibrational levels without having to describe the relaxation processes among them explicitly. Moreover, our ab initio theory accurately captures the interplay of millions of population degrees of freedom in the laser, including many collisional processes that other researchers neglected or approximated, such as inhomogeneous broadening, dipole–dipole collisions, symmetry-preserving thermalization, V-swap processes, molecule–wall collisions, velocity subclasses, and spatial diffusion. An efficient numerical solver is developed to find the steady state directly, without time evolution, as a system of millions of coupled nonlinear rate equations. Not only does the model match experiments; it also unexpectedly shows that our compact laser exhibits remarkable conversion efficiency, up to 39% of the Manley–Rowe (23) limit. Our compact laser is 1,000× smaller in volume while delivering more than

Significance

Optically pumped far-infrared (OPFIR) lasers are one of the most powerful continuous-wave terahertz sources. However, such lasers have long been thought to have intrinsically low efficiency and large sizes. Moreover, all previous theoretical models failed to predict even qualitatively the experimental performance at high pressures. Here, we have developed an innovative model that captures the full physics of the lasing process and correctly predicts the behavior in the high-pressure regime. Validated against experiments, our model shows that nearly all previous OPFIR lasers were operating in the wrong regime and that 10× greater efficiency is possible by redesigning the terahertz cavity. Our results reintroduce the use of OPFIR lasers as a powerful and compact source of terahertz radiation.

ENGINEERING

A waveguide cavity filled with $^{13}CH_3F$

improved design for TE$_{01}$ mode

L=14.3cm

movable back reflector

R=0.25cm

IR in

r=0.5mm

front window with a pinhole

focus mirror

THz out

detector

B $^{13}CH_3F$

Energy (cm^{-1})

vibrational thermal pools

$V_{\Sigma}A$ | $V_{\Sigma}E$

V_3A thermal pool

K=3

J=11

J=6
J=5 — U
J=4 — U−1
J=3

pump

2000

V_6

V_3 — 1000

V_0A thermal pool

K=3
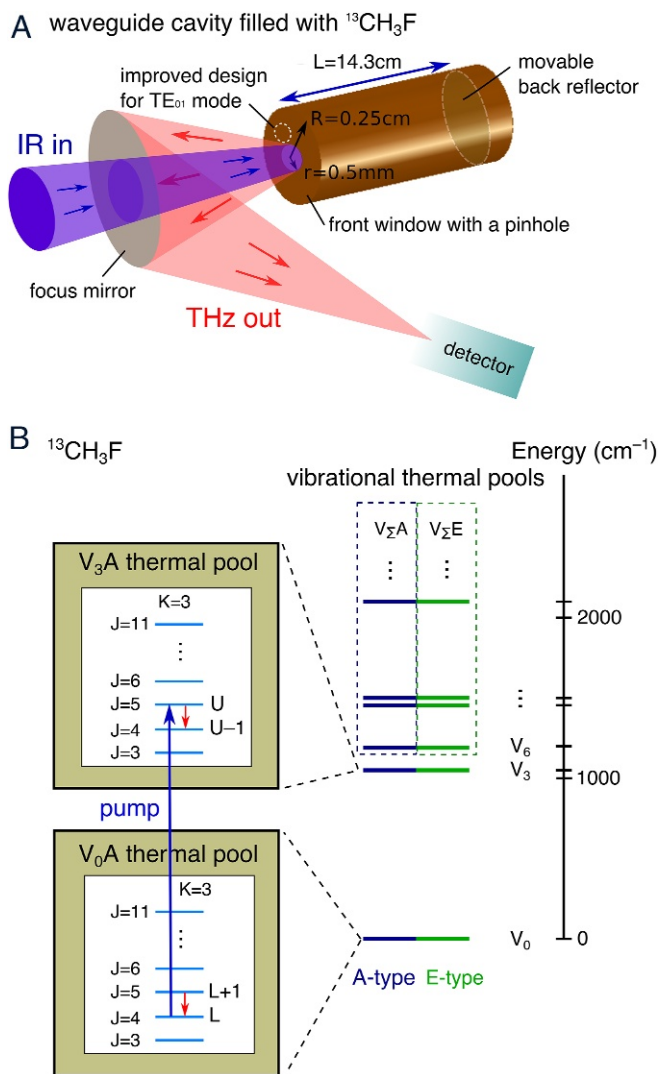
J=11

J=6
J=5 — L+1
J=4 — L
J=3

V_0 — 0

A-type E-type

Fig. 1. (*A* and *B*) Schematics of (*A*) the laser cavity and (*B*) molecular energy levels of $^{13}CH_3F$. The cavity is a copper tube with a movable back wall used to tune the cavity frequency to match the laser gain, pumped with an IR laser through a pinhole in the front window. The energy levels consist of vibrational levels V_ℓ, with A and E symmetries (10), composed of rotational levels with quantum numbers J and K. The IR pump excites a transition between levels L and U as shown, and lasing occurs for both the direct inversion between U and U − 1 and the refilling inversion between L + 1 and L.

10× greater efficiency than the best commercial OPFIR lasers (Fig. 3). Finally, we explore and optimize the cavity geometry (Fig. 4) to achieve even greater output terahertz power over a much wider range of gas pressures. We believe that these findings will revive interest in OPFIR lasers as high-power, compact, continuous-wave terahertz sources.

Experimental Measurements

Fig. 1 depicts our OPFIR laser: A line-tunable CO_2 pump laser ($\lambda = 9.7\mu m$) is focused through a pinhole in the front copper mirror into a 5-mm × 14.3-cm copper tube filled with $^{13}CH_3F$ gas. The lasing transition is brought into resonance with the cavity by a copper-plunger rear mirror that adjusts the cavity length, and the resulting laser power emerges from the same pinhole, after which it is detected by a heterodyne receiver. The different rotational levels are characterized by a rotational quantum number J, its projection quantum number K, and the vibrational state V_ℓ to which it belongs (24, 25). For symmetric-top molecules,

there are two nuclear spin-dependent symmetry types, A and E (10, 24). In $^{13}CH_3F$, the coincidence between the 9P(32) line of the pump laser and the $R_3(4)$ ro-vibrational transition in $^{13}CH_3F$ produces two rotational population inversions, the "direct" $J = 5 \rightarrow 4$ (with $K = 3$, type A) inversion in V_3 with frequency 245.351 GHz and a corresponding "refilling" rotational transition in the type A ground vibrational level V_0 with frequency 248.559 GHz (Fig. 1) (13). The heterodyne receiver distinguishes the lasing transitions and measures their intensity as a function of pressure and the input pump power. Fig. 2 shows that the refilling transition produces the most terahertz power in a manner that depends nonlinearly on the input pump power, but the direct inversion survives over a much broader range of pressures. In contrast with previous theoretical models that predicted a pump power-independent vibrational bottleneck, these pressure-dependent and pump power-dependent behaviors in our compact OPFIR laser show no vibrational bottleneck on either transition. In fact, increasing pump power produces higher-pressure operation, indicating even stronger emission and higher pressures are achievable.

Ab Initio Modeling

To understand the lack of vibrational bottlenecking, a thorough model of OPFIR laser operation must capture many different physical processes. Gas-phase molecules typically have hundreds to thousands of thermally populated rotational energy levels in the same vibrational modes as the pumped states ($L \rightarrow U$). It has previously been shown that rapid collisional thermalization maintains a Boltzmann distribution of population across most rotational states within a given vibrational level V_ℓ and symmetry type (A or E); consequently, they may be modeled as a thermal pool (5, 8–10). This thermal-pool approximation dramatically simplifies models of the collision physics by reducing the number of levels that must be individually included and collision cross-sections that must be known to those few most closely connected to L and U. Nevertheless, after the pump excites molecules from L to U, a complicated set of collisional relaxation processes ensues, both bimolecular rotational energy transfer and molecular diffusion to the walls for ro-vibrational thermalization, so that population inversions between L + 1 and L (refilling) and U and U − 1 (direct) occur in a manner that depends sensitively on the input pump power, pressure, radial population distribution, cavity length, and cavity mode. Because wall collisions are the primary pathway for vibrational relaxation in OPFIR lasers and the diffusion rate goes as $1/pR^2$ for pressure p and cell radius R, typical large-diameter glass OPFIR lasers require operation at low pressure, while small-diameter metallic cells are favored for high-pressure operation (with the tradeoff of increased ohmic losses at the lasing frequency).

Various models have been developed in an attempt to understand the inversion process (2–4, 13). A troubling limitation in all these models, shown in *SI Appendix*, Fig. S2, was that they exhibited an unphysical bottlenecking of the inversion at high pressures, regardless of the input pump power. Consequently, they were unable to explain high-pressure lasing such as that shown in Fig. 2. Ref. 7 addressed the problem of high-pressure bottlenecking by including more vibrational levels; however, that model was too oversimplified and incomplete to provide useful quantitative guidance for cavity design, and the lack of an efficient numerical solver prohibited any attempt at a more realistic model.

Retaining the spirit of ref. 7, we construct a far more complete model that quantitatively describes how this unphysical bottlenecking is overcome through the collisional excitation of molecules into hundreds of excited vibrational levels in compact OPFIR lasers. In our model, whose complete mathematical details are provided in *SI Appendix*, section 1: Experimental Measurements and Theoretical Modeling, the degrees of
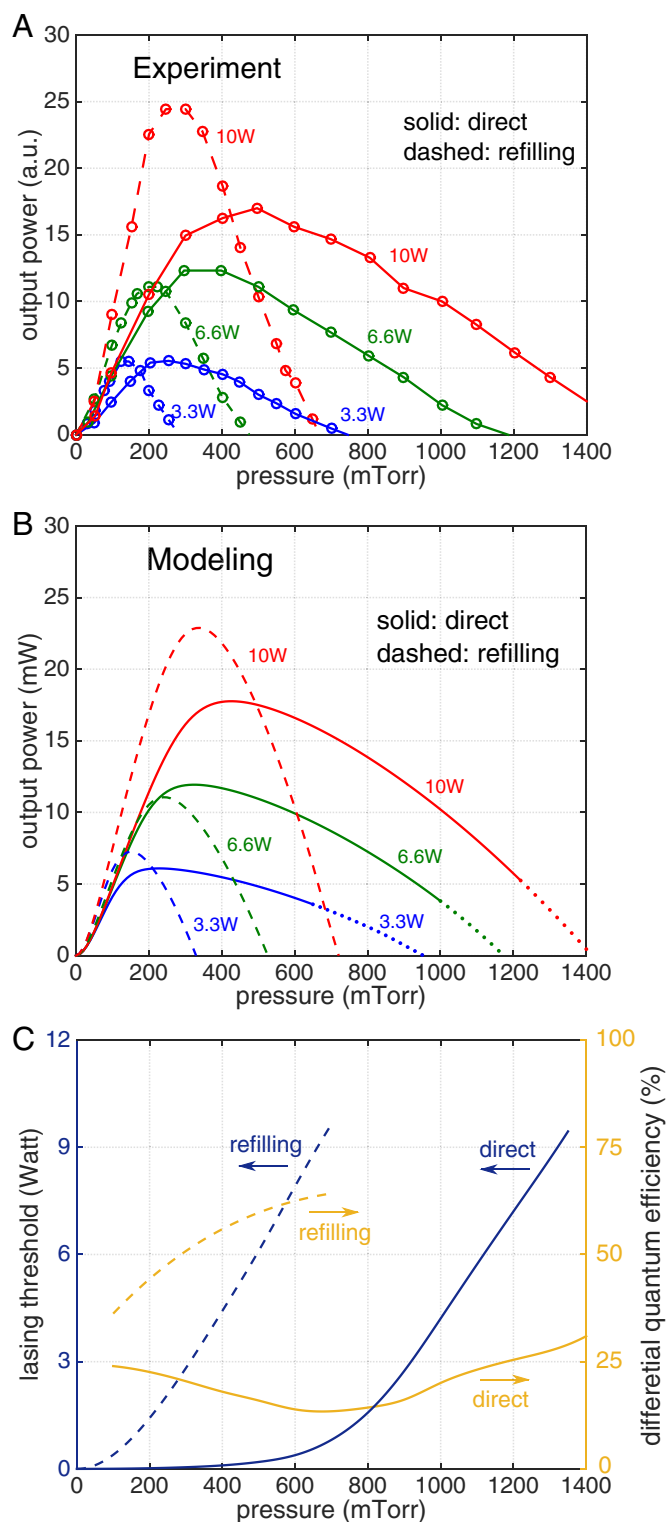
Fig. 2. (*A*) Experimental and (*B*) theoretical terahertz laser output power as a function of gas pressure, for various input pump powers (3.3 W, 6.6 W, and 10 W) and for both the direct (solid lines) and refilling (dashed lines) transitions. Excellent agreement is obtained even though the theoretical model has no adjustable parameters; in contrast to previous work (2–4, 13), our theory captures the fact that higher powers allow operation at higher pressures, in part because of an innovative technique to model a large number of high-energy vibrational levels. The dotted parts of the direct lasing curves represent an inefficient regime in which the pump intensity is nearly zero in the back of the cavity. In this case our model's approximation of an effective z-uniform pump strength is inaccurate, but it is not desirable to operate in

freedom in the rate equations include axial molecular speed v, radial position r, time t, and different energy levels including nonthermal rotational levels and vibrational thermal pools. By calculating separate populations at each v, unlike previous work, we can accurately model inhomogeneous broadening and spectral hole burning (SHB) effects on the Doppler-broadened pumped IR transition and the resulting pressure-broadened terahertz gain profile. By additionally modeling each population density as a function of r, the overlap between the inversion and the cavity mode is calculated for an accurate estimation of the weighted gain coefficient. In the efficient regime where the pump intensity reaches the entire cavity (i.e., IR absorption, spectral hole burning, and saturation effects do not cause the pump intensity to decay strongly before reaching the end of the cavity), the populations can be approximated as uniform in z with an effective z-averaged pump intensity (different from the input pump intensity, *SI Appendix*, section 2: More Technical Details), which greatly simplifies the calculations.

Given a set of nonlinear rate equations, most authors evolve them in time until the steady state is obtained (9, 13), but this approach is severely inefficient, especially at high pressures where timescales for different relaxation processes diverge widely. Instead, we solve for the steady state directly, without time evolution, as a system of millions of coupled nonlinear equations, with computational cost equivalent to less than 100 time-evolution steps. This enormous computational improvement allows us to include not only millions of population degrees of freedom but also many physical processes that other authors neglected or approximated. In particular, we include dipole–dipole collisions between rotational states (12), symmetry-preserving thermalization (SPT) (also called K-swap processes) between nonthermal rotational states and vibrational thermal pools, the V-swap process (10, 24), nonresonant collisions among thermal pools (24, 25), molecule–wall collisions (9, 13), and spatial diffusion (13). For the inhomogeneously broadened pump absorption (25), we include Doppler, AC-Stark (26), and pressure (23) broadening of velocity subclasses, and we determine the average pump intensity self-consistently, including SHB and pump saturation, with the absorption coefficient calculated from the populations. Given rate equations for the populations $N_k(v, r, t)$ of each level k (*SI Appendix*, section 1: Experimental Measurements and Theoretical Modeling), by setting $\partial N_k/\partial t = 0$ we obtain a nonlinear system of equations for the steady-state populations $N_k(v, r)$. From the calculated radially dependent population inversions, gain profiles, and lasing mode geometry, the output of the model is the predicted lasing power I_o, calculated using modified standard formulas (23) with a self-consistent characteristic time as described in *SI Appendix*, section 1: Experimental Measurements and Theoretical Modeling.

Even with the thermal pool simplification and steady-state computation efficiency, the sheer complexity of the inversion process makes it extremely challenging to model accurately. Previous models needed to make many simplifying assumptions, and the reason they produced unphysical bottlenecking at high pressures was conjectured to be their inclusion of only two key vibrational levels (7, 9), e.g., V_0 and V_3 for $^{13}CH_3F$. We confirmed this conjecture with our model by artificially "turning off" collisional processes one by one. The only process that circumvented vibrational bottlenecking was the process by which higher-lying vibrational levels are populated. The difficulty of including these higher-lying vibrational levels seems almost

this regime. Our model also predicts (*C*) the input pump power at lasing threshold (blue) and the differential quantum efficiency (DQE) (yellow) (23) normalized by the Manley–Rowe (MR) limit at threshold vs. pressure for both inversions. The refilling inversion is both higher power and higher efficiency, with a modeled DQE that can reach 64%.
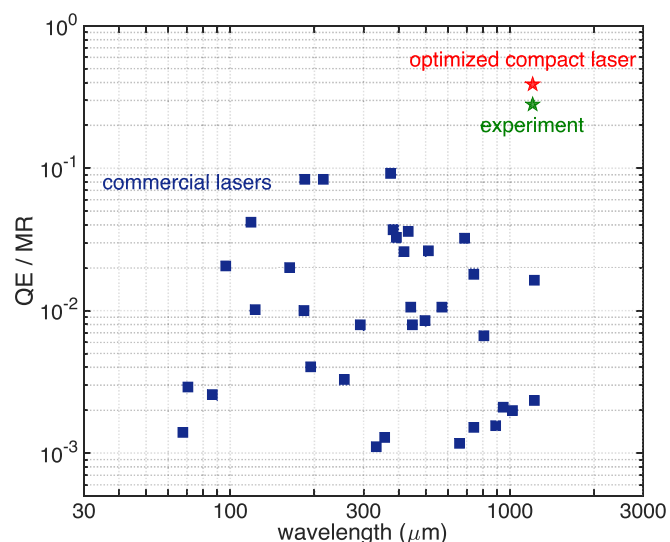
Fig. 3. Total quantum efficiency (23) (QE = THz power out/IR power in) of commercial OPFIR lasers (https://www.edinst.com/products/) and our compact OPFIR laser, normalized by the MR limit (23) on QE. Our experimentally demonstrated laser achieves a QE that is 29% of the MR limit (29% of 0.8%) which improves to 39% after cavity optimization. Both are 10× better than the best commercial laser at the same frequency (0.25 THz or 1.2 mm wavelength), while being 1,000× smaller—in fact, we show theoretically that this efficiency boost is mainly due to the fact that our cavity is so much smaller.

insurmountable at first: Although the energies of hundreds of vibrational levels are known (25), the relaxation processes among them are not known quantitatively and are infeasible to measure. To deal with that problem, a crucial theoretical innovation of our work is to describe those levels implicitly via an effective temperature (different from the ambient temperature!) that is determined self-consistently from the few collisional cross-sections whose values are known. Specifically, we make the ansatz that vibrational transitions are rapid enough to "thermalize" those levels with a Boltzmann distribution described by an effective temperature T_v, so they may be grouped together into separate population pools V_Σ for the A and E symmetries, as shown in Fig. 1B. This is similar to the experimentally justified thermal-pool assumption (8, 10) that maintains a constant temperature among rotational states within a given symmetry type and vibrational level. The main justification of this ansatz is that thermalization among vibrational states is through bimolecular collisions, meaning the rates increase with pressure, while vibrational-state relaxation occurs through diffusion to the walls, which goes as the inverse of pressure. Therefore, the higher the pressure, the more vibrational thermalizing collisions occur before diffusion to the walls relaxes the excitation, and so our model becomes more accurate precisely in the high-pressure regime where these extra vibrational levels are relevant to the inversion.

To implement this thermalization ansatz, the populations of V_0 and V_3 are calculated explicitly, and we then assign the effective temperature of the remaining vibrational levels to be $T_v = (E_{V_3} - E_{V_0})/k_B \log(N_{V_3}/N_{V_0})$, where E_{V_ℓ} and N_{V_ℓ} are the energy and population of level V_ℓ. T_v must be determined self-consistently by our nonlinear solver, simultaneously with N_{V_3} and N_{V_0}, because any population assigned to N_{V_Σ} according to T_v is removed from N_{V_3} and N_{V_0}. If we replace these effective vibrational levels with an explicit six-level model [or even a three-level model as in previous work (2–4, 13)], but include all of the other processes of our model, we find the return of the vibrational bottleneck as in previous work: The inversion disappears above 700 mTorr for all input pump powers

(*SI Appendix*, Fig. S2). Therefore, we confirm the conjecture that including a complete set of vibrational levels through V_Σ eliminates high-pressure bottlecking. Indeed, Fig. 2 shows excellent agreement between the experimentally measured power (Fig. 2*A*) and the predictions of our model (Fig. 2*B*), with no free parameters except for the overall scaling, even for pressures >1 Torr where previous models exhibited bottlenecking. In comparing the experimental results to the theoretical model, it is important to keep in mind that there are significant experimental variabilities that limit reproducibility. Among the largest sources of variability are $\sim \pm 10$-MHz drift in the pump frequency offset, $\sim \pm 2$-μm drift in cavity length from the optimal for a given terahertz inversion, and $\sim 10\%$ rise in the cavity pressure over the course of a measurement. A final source of variability is that the optimal tuning for the refilling transition is different from that for the direct transition. Given these
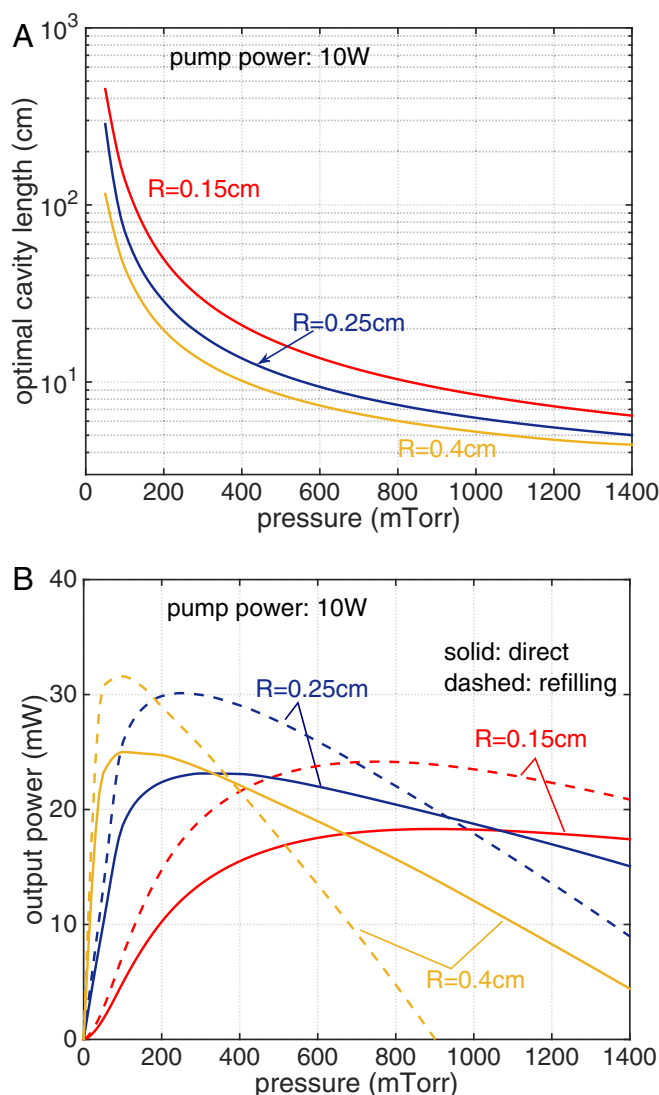

Fig. 4. Theoretical predictions of (*A*) the roughly optimal cavity length for various radii and (*B*) the optimized laser output power, both as a function of pressure for an input pump power of 10 W. The cavity length is optimized to equal half the decay length of the pump beam. The output power (*B*) is shown for the optimal cavity length at each pressure and radius so that each data point is a separate cavity design. The peak efficiency is increased from 29% of MR in the experimental cavity to 39%, but more importantly this optimization allows efficient operation at a wider range of high pressures and hence in smaller cavities.

variabilities, the excellent, roughly quantitative agreement with our model provides striking confirmation of its validity (Fig. 2).

In the dotted parts of Fig. 2*B*, the pump is highly focused in the front of the cavity and quickly decays to nearly zero (<2%) by the back of the cavity, in which case our model's approximation of an effective *z*-uniform pump strength is inaccurate, and hence the slight mismatch with experiment is unsurprising. Accurately modeling this attenuated-pump regime is relatively unimportant because, as described below, that regime "wastes" the end of the cavity, and it is preferable to use a shorter cavity.

Since the lasing-mode pattern could not be observed directly in the experiment, we compute the terahertz cavity loss (*SI Appendix*, section 1: Experimental Measurements and Theoretical Modeling) from the lowest-lost [TE$_{01}$ (27)] mode for all curves except for the refilling lasing with input pump power 6.6 W. The 6.6-W experimental refilling curve exhibited a jump in amplitude compared with adjacent powers. We deduce that this is due to a different mode being excited by a mistuned cavity—using the cavity loss and mode profile from the TE$_{22}$ mode produced the best fit to the data. In this way, the accuracy of the model enables us to determine which mode is lasing without directly measuring the mode profile.

Operating OPFIR laser sources at high pressures also leads to an unusually broad and flat gain profile, as shown in *SI Appendix*, Fig. S6. The width of this pressure-broadened gain profile is proportional to the gas pressure (23), as described in *SI Appendix*, section 2: More Technical Details. Such flat gain profiles potentially allow the terahertz lasing frequency to be tuned over a correspondingly broad range ($\sim \pm 10$ MHz at a few hundred millitorrs) without sacrificing efficiency.

Lasing Efficiencies

The agreement between theory and experiment allows us to use the theory to assess the attainable quantum efficiency of the laser accurately and quantitatively, a parameter which was difficult to measure in our experiment because only a fraction of the emitted photons were detected by our heterodyne receiver (*SI Appendix*, section 1: Experimental Measurements and Theoretical Modeling). Fig. 2*C* plots the predicted lasing threshold and DQE at the threshold, defined as $\eta_d = \frac{dP_{\text{out}}}{dP_{\text{pump}}} / \frac{\nu_{\text{out}}}{\nu_{\text{pump}}}$. Fig. 2*C* shows that the direct transition has a lower pump threshold, but its DQE is smaller than the refilling transition (which can reach as high as 64%). We also obtain the total quantum efficiency (QE), defined as $\eta_t = \frac{P_{\text{out}}}{P_{\text{pump}}} / \frac{\nu_{\text{out}}}{\nu_{\text{pump}}}$, which is theoretically bounded by 100% from the MR limit (23): The highest achievable power conversion efficiency is the ratio of output and pump frequencies. Our computed QE can be as high as 29% at 350 mTorr for the refilling transition and, as explained below, can increase to 39% in an optimized cavity. As shown in Fig. 3, both QE values are considerably larger than those attained in previous commercial OPFIR lasers.

The remarkably high QE and DQE are an unexpected benefit of high-pressure operation, especially for the refilling transition. The model indicates that as pressure increases, T_v also increases as more of the pumped molecules are collisionally transferred from V$_3$ to V$_\Sigma$ and are therefore removed from the V$_0$ and V$_3$ A-type thermal pools that quench the refilling and direct inversions, respectively. DQE measures the likelihood that each additional pump photon just above threshold produces an additional terahertz photon, and the high DQEs seen at the highest operational pressures mean that both inversions are increasingly efficient as bottlenecking traps molecules in higher vibrational levels. In other words, below threshold most pumped molecules are quickly lost from the levels associated with the inversions due to rapid collisional thermalization, but just above threshold for a given pressure, sufficient collisional redistribution and equilibration of population have been achieved that additional

pump photons simply add to the strength of the inversions. This is particularly true for the refilling transition, where the inversion with L + 1 is produced as the pump laser removes molecules from L. The efficiency of the direct transition is lower and less sensitive to pressure because the pumped molecules placed in U are quickly removed by collisional processes. Consequently, the model indicates that it is the refilling transitions, not the direct transitions typically used in traditional OPFIR lasers, that are most attractive for compact, high-pressure, efficient OPFIR lasers.

Cavity Optimization

With this full understanding of the lasing physics at all pressures, we can finally explore and optimize the cavity geometry to maximize the THz power for compact OPFIR lasers. In particular, we consider the choice of cavity length and radius. Performing parameter variation with our model indicates that output power is maximized by a cavity length of roughly $1/2\alpha_p$, where α_p is the average pump absorption coefficient (*SI Appendix*, section 2: More Technical Details), so here we define $L_o = 1/2\alpha_p$ to be the "optimal" cavity length. Fortunately, operating with this cavity length also ensures the validity of our *z*-averaged pump-intensity approximation, since L_o is several times smaller than the length where this approximation begins to fail due to nonuniform pump intensity. Calculating L_o is nontrivial because α_p itself depends on cavity length (*SI Appendix*, section 2: More Technical Details), so L_o must be obtained by a self-consistent nonlinear search.

Fig. 4*A* shows the optimal cavity length as a function of pressure with three different radii R= 0.15 cm, 0.25 cm, and 0.4 cm, with pump power set at 10 W. Because pump absorption increases with increasing pressure, we can see that higher pressures favor shorter cavities. The increase in optimal cavity length with decreasing cavity diameter derives from the increasing pump intensity, the associated increase in AC-Stark broadening and SHB, and the increasing saturation of the pumped L → U transition for a given input pump power. Given that our cavity length was maintained at approximately 14.3 cm for all our measurements, the model indicates that the experimental drop in OPFIR laser power with increasing pressure is caused in part by excess cavity length and incomplete pumping of the entire volume. Another design improvement can be achieved by placing the front pinhole at an optimized position: One chooses the pinhole location to increase the output flux of the lasing mode, which increases both the output power and the efficiency by decreasing the fraction of power lost to ohmic absorption. For example, the TE$_{01}$ mode (27) has a maximum flux intensity around $r = 0.48R$, so an off-center pinhole will achieve larger lasing power, as shown schematically in Fig. 1*A*. We compute the effect of the pinhole location by calculating the TE$_{01}$ flux through the hole in *SI Appendix*, section 2: More Technical Details.

With the input pump power set at 10 W, the predicted output power for cavities of optimized length and pinhole position is shown in Fig. 4*B*. Comparison with Fig. 2 *A* and *B* indicates how severely the high-pressure lasing is hampered by excess cavity length. For optimized cavities, the maximum output power can reach 31 mW, which is 39% of the MR limit. Cavities with a larger radius of $R = 0.4$ cm can achieve slightly higher output power at low pressures (around 100 mTorr). However, low pressure indicates longer cavity length (around 50 cm) from Fig. 4*A*. In contrast, 0.15-cm diameter cavities shorter than 20 cm can generate output power about 25% of the MR limit in a wide range of pressure above 400 mTorr. This requirement for widely adjustable cavity lengths is in stark contrast to traditional fixed-geometry OPFIR lasers, typically 10 cm in diameter and 1 m in length (https://www.edinst.com/products/). Our analysis explains why these huge cavities are inefficient, can operate only at very low pressures, and may not be long enough!

Concluding Remarks

Our compact laser is $1{,}000\times$ smaller in volume while delivering $10\times$ greater efficiency than previous OPFIR lasers at this wavelength. This is shown in Fig. 3, where the QE normalized by the MR limit is plotted for both our experimental setup and our optimized compact laser, as well as for the best commercial OPFIR lasers. The MR limit indicates that for a given input pump power and quantum efficiency, output power increases linearly with decreasing lasing wavelength, so our analyses suggest that future OPFIR lasers can produce even higher powers with a careful choice of cavity and gas. Moreover, we have only scratched the surface of the design possibilities offered by our ability to model the full physics of OPFIR lasers accurately, and we believe that many further discoveries await the extension of our approach to other gases (such as CO and N_2O, e.g., for other wavelengths), other transitions (e.g., for line-tunable operation), and other cavity designs.

Materials and Methods

The experimental procedure, as depicted in Fig. 1 and described in more detail in *SI Appendix*, section 1: Experimental Measurements and Theoretical Modeling, used a sealed 14.3×0.5-cm OPFIR laser cavity, filled with $^{13}CH_3F$ gas, that was pumped by a CO_2 laser at $\lambda = 9.657$ μm. For each pump power and pressure, a copper plunger in the rear of the tube was adjusted to tune the terahertz cavity resonance to either the direct or the refilling transition, and the resulting terahertz emission was measured by a heterodyne receiver.

Our theoretical model consists of a set of rate equations giving $\dot{N} = \partial N/\partial t$ for both nonthermal rotational populations N^r_ℓ and nonequilibrium populations of vibrational thermal pools N^v_ρ. The theoretical goal is to predict these differences N from the equilibrium (unpumped) populations and their consequences for terahertz gain. In *SI Appendix*, section 1: Experimental Measurements and Theoretical Modeling, these rate equations (which include various transitions, coupling to the pump, diffusion, and an effective-temperature model for unknown vibrational levels), how the $\dot{N} = 0$ steady state is found, and finally how the output power is extracted self-consistently from the populations are discussed in detail.

1. Chang TY, Bridges TJ (1970) Laser action at 452, 496, and 541 μm in optically pumped CH_3F. *Opt Commun* 1:423–426.
2. Hodges DT, Tucker JR, Hartwick TS (1976) Basic physical mechanisms determining performance of the CH_3F laser. *Infrared Phys* 16:175–182.
3. Henningsen J, Jensen H (1975) The optically pumped far-infrared laser: Rate equations and diagnostic experiments. *IEEE J Quantum Electron* 11:248–252.
4. Dangoisse D, Glorieux P, Wascat J (1981) Diffusion and vibrational bottleneck in optically pumped submillimetre lasers. *Int J Infrared Millimeter Waves* 2:215–229.
5. Matteson W, De Lucia F (1983) Millimeter wave spectroscopic studies of collision-induced energy transfer processes in the $^{13}CH_3F$ laser. *IEEE J Quantum Electron* 19:1284–1293.
6. Tobin MS (1985) A review of optically pumped NMMW lasers. *Proc IEEE* 73:61–85.
7. Everitt HO, Skatrud DD, De Lucia FC (1986) Dynamics and tunability of a small optically pumped cw far-infrared laser. *Appl Phys Lett* 49:995–997.
8. McCormick RI, De Lucia FC, Skatrud DD (1987) A time-resolved study of rotational and vibrational excitation and relaxation in the $^{13}CH_3F$ optically pumped far-infrared laser. *IEEE J Quantum Electron* 23:2060–2068.
9. McCormick RI, Everitt HO, De Lucia FC, Skatrud DD (1987) Collisional energy transfer in optically pumped far-infrared lasers. *IEEE J Quantum Electron* 23:2069–2077.
10. Everitt HO, De Lucia FC (1989) A time-resolved study of rotational energy transfer into A and E symmetry species of $^{13}CH_3F$. *J Chem Phys* 90:3520–3527.
11. Douglas NG (1989) *Millimetre and Submillimetre Wavelength Lasers: A Handbook of CW Measurements* (Springer Berlin), Vol 61.
12. Everitt HO, De Lucia FC (1990) Rotational energy transfer in CH_3F: The $\Delta J = n$, $\Delta K = 0$ processes. *J Chem Phys* 92:6480–6491.
13. Chua SL, et al. (2011) Spatio-temporal theory of lasing action in optically-pumped rotationally excited molecular gases. *Opt Express* 19:7513–7529.
14. Tonouchi M (2007) Cutting-edge terahertz technology. *Nat Photon* 1:97–105.
15. Ferguson B, Zhang XC (2002) Materials for terahertz science and technology. *Nat Mater* 1:26–33.
16. Siegel PH (2002) Terahertz technology. *IEEE Trans Microwave Theory Tech* 50:910–928.
17. Button KJ (2013) *Reviews of Infrared and Millimeter Waves: Optically Pumped Far-Infrared Lasers* (Springer Science & Business Media, New York), Vol 2.
18. Johnson A, Auston D (1975) Microwave switching by picosecond photoconductivity. *IEEE J Quantum Electron* 11:283–287.
19. Van Exter M, Grischkowsky D (1990) Optical and electronic properties of doped silicon from 0.1 to 2 THz. *Appl Phys Lett* 56:1694–1696.
20. Andronov AA, et al. (1978) The gyrotron: High-power source of millimetre and submillimetre waves. *Infrared Phys* 18:385–393.
21. Faist J, et al. (1994) Quantum cascade laser. *Science* 264:553–555.
22. Williams BS (2007) Terahertz quantum-cascade lasers. *Nat Photon* 1:517–525.
23. Saleh BEA, Teich MC (1991) *Fundamentals of Photonics* (Wiley, New York), Vol 22.
24. Everitt HO, De Lucia FC (1995) Rotational energy transfer in small polyatomic molecules. *Adv At Mol Opt Phys* 35:331–400.
25. Everitt HO, III (1990) Collisional energy transfer in methyl halides. PhD thesis (Duke University, Durham, NC).
26. Panock R, Temkin R (1977) Interaction of two laser fields with a three-level molecular system. *IEEE J Quantum Electron* 13:425–434.
27. Bansal R (2006) *Fundamentals of Engineering Electromagnetics* (CRC Press, Boca Raton, FL).